Pair-creation collective modes in an electron gas

P. Pulsifer* and G. Kalman
Department of Physics, Boston College, Chestnut Hill, Massachusetts 02167
(Received 22 October 1991)

High-energy modes of oscillation in a zero-temperature relativistic electron gas in a strong background magnetic field are reported. The modes propagate parallel to the magnetic field and appear both in a longitudinal and in two transverse polarizations. The underlying mechanism is the binding between electrons near the Fermi surface and virtual positrons, which is enhanced by the presence of the filled Fermi distribution, in a Cooper-pair-like phenomenon. The energy of the mode is of the order of the pair energy (over 1.02 MeV), and the mode exists only for wave numbers k above a critical value, such that the mode group velocity exceeds the velocity of an electron on the Fermi surface. Damping of the mode is insignificant at the critical wave number and increases with k to a relatively small maximum value.

PACS number(s): 52.25.Mq, 52.60.+h, 12.20.Ds, 97.60.Jd

I. INTRODUCTION

In this paper we report the investigation of relativistic modes of collective excitation in a zero-temperature electron gas, propagating parallel to a strong background magnetic field. This report arises from a more general investigation of wave propagation in such a system [1]. The high-frequency modes are connected with the process of virtual pair production: The mode energy $\hbar\omega$ is very nearly the energy of an electron-positron pair created with total momentum $\hbar k$ and with the electron on the Fermi surface; the modes are damped by real pair production. There is a triplet of modes, for different polarizations, associated with each occupied Landau level (except for the 0th level, which carries only two modes). Each mode exists only above a critical wave number, of order $2p_s$, where p_s is the Fermi momentum associated with level s. This critical wave number could be close to zero, for a nearly empty level, or could be very large, for a full level in a dense system. The critical wave number marks the k value above which the group velocity of the mode exceeds the electron Fermi-surface velocity; also, at this critical value, the virtual electron and positron move with equal velocities. Damping of the modes is nonzero, due to vacuum polarization effects, but becomes vanishingly small near the critical wave number. The damping grows as the wave number increases from the critical value (and the electron-positron relative velocity increases), until a maximum is reached; thereafter, the damping decreases with wave number (though this decrease may occur beyond the limits of the theory). For the cases presented here, damping is not very significant.

The present analysis applies to a system consisting of a degenerate electron gas, dense enough so that the Fermi energy is at least a substantial fraction of the electron rest mass. The system is immersed in a strong uniform magnetic field, so that the quantization of electron motion transverse to the field is significant and the energy of the Landau-level separation can be comparable to the electron rest-mass energy. Under these conditions the motion of the electrons is quasi-one-dimensional and the singularities appearing in the response function are stronger than in the three-dimensional case.

The physical mechanism responsible for the generation of the modes can be viewed as the binding of virtual electron-positron pairs from the vacuum, made possible by the presence of the background high-density electron gas. Normally, the virtual electrons and positrons emerging from the vacuum do not bind, despite their electrostatic attraction. One case where they do is in the presence of an "ultrastrong" magnetic field, $B > 1.6\times 10^{16}$ G, where a boson excitation in the form of a massive longitudinal photon has been reported [2]. In the case described here, the high-density degenerate electron background enhances the binding of the virtual pair, making binding possible for any value of the magnetic field, although the strength of the resulting excitation is still a sensitive function of the magnetic-field strength. The electron-positron binding is then the result of a Cooper-pair-like phenomenon: The Coulomb interaction is enhanced by virtue of a large portion of the momentum space being unavailable to the electron. The scenario is similar to that of Bethe and Goldstone [3], except that there both interacting particles were within the Fermi sea, whereas here, the electron is outside, on the Fermi surface, and the positron is unaffected by the phase-space exclusion. A more direct analogy is the formation of the Mahan excitons [4] in metals, by creation of a deep-lying core hole and the lifting of an electron above the Fermi surface. The formal manifestation of these phenomena is the appearance of a sharp logarithmic peak in the response function [3], which provides new solutions of the dispersion equation.

The results given here are derived from a kinetic study of a relativistic degenerate electron gas [1], which uses the linearized Vlasov equation for the Wigner distribution function to compute the current response to a perturbation in the electromagnetic four potential, and in this way calculates the polarization tensor for the system. The calculation is done in the random-phase approximation; as discussed below, the present theory should be at least qualitatively valid for $k < n^{1/3}$ and $r_s \ll 1$, where r_s

is the conventional coupling parameter, equal to the interparticle distance divided by the Bohr radius; the precise condition on r_s depends on the magnetic field and is given below. Pair-production modes are most likely to exist in astronomical objects such as neutron stars, which are both highly degenerate and highly magnetized, but conditions for their existence could also possibly be satisfied on earth.

The plan of this paper is as follows. In Sec. II we sketch the formalism used to describe the behavior of the relativistic magnetized electron gas under disturbances of arbitrary frequency and wavelength. Section III discusses the dispersion relation in this system for waves propagating along the magnetic field, and describes the characteristics of the pair-creation modes. In Sec. IV we estimate the validity of the approximations employed.

II. FORMALISM

Wave propagation and collective modes in a dense relativistic plasma have been studied by a number of authors, usually by calculating a response function such as the dielectric, conductivity, or polarization tensors. The dispersion relation for collective modes $\omega(k)$ is written in terms of this response function. For the present work, the Wigner-function kinetic equation method [1,5] was employed; other response-function calculations have used the Green-function [6–8] or density-matrix [9,10] techniques, or some variant of these [11]. Previous studies of the full (k,ω)-dependent response function have mostly been restricted to the long-wavelength, low-frequency (relative to the rest mass) regime. For calculating the relativistic response, a Green-function method has been applied [7,8], but explicit results were shown only for the $\omega=0$ and $k=0$ situations. Our calculations [1], which form the basis for this paper, have explicitly displayed the full (k,ω)-dependent response function for a relativistic system.

The polarization tensor $\Pi_{\mu\nu}(k,\omega)$ is a response function that links the four current to the electromagnetic potential:

$$J_\mu(k,\omega)=\Pi_{\mu\nu}(k,\omega)A^\nu(k,\omega)\ . \tag{1}$$

This expression is gauge invariant, because $\Pi^{\mu\nu}k_\mu=\Pi^{\mu\nu}k_\nu=0$. The polarization tensor is related to the four-dimensional dielectric tensor $\epsilon_{\mu\nu}(k,\omega)$ as follows:

$$\epsilon_{\mu\nu}(k,\omega)=1-\frac{4\pi\Pi_{\mu\nu}(k,\omega)}{\omega^2}\ . \tag{2}$$

The covariant dispersion relation determining wave propagation in the plasma is

$$\det|k^\alpha k_\alpha g_{\mu\nu}-k_\mu k_\nu+4\pi\Pi_{\mu\nu}|=0\ , \tag{3}$$

where $g_{\mu\nu}$ is the Minkowskian metric tensor. When only propagation parallel to the magnetic field is considered, the wave vector becomes $k^\mu=(\omega,0,0,k)$, and Eq. (3) simplifies.

The polarization tensor can be separated into two parts, one depending on particle distribution functions (the particle part) and one independent of particle distribution functions (the vacuum part). The vacuum part $\Pi^0_{\mu\nu}(k,\omega)$ has been calculated for parallel propagation by Bakshi, Cover and Kalman [7]. It has two independent elements, Π^0_{33} and $\Pi^0_{11}=\Pi^0_{22}$, which are functions of the relativistic invariant ω^2-k^2. The vacuum polarization is a slowly changing function, small compared to unity except for peaks at the frequencies $\omega_{\min}$ discussed below.

In order to see the qualitative features associated with the particle part of $\Pi_{\mu\nu}(k,\omega)$, we will first discuss the properties of the relativistic, strongly magnetized system, particularly with regard to the kinematics of pair production. We will then discuss the properties of the polarization tensor $\Pi_{\mu\nu}(k,\omega)$ in the ω-k plane, and consider the high-frequency waves described by this response function, with their dispersion relation $\omega(k)$ and damping. Henceforth, we work in Gaussian units, with $\hbar=c=1$. In numerical formulas B is given in units of gauss and the electron density n in cm^{-3}; energies and momenta are given in terms of the electron mass m.

In a strongly magnetized system, electron motion perpendicular to the field is quantized into Landau levels, with integral quantum number $s\geq 0$. The relativistic electron energy is given by

$$\varepsilon_{ps}=(a_s^2+p^2)^{1/2}\ , \tag{4}$$

where p is the momentum parallel to the field, and where

$$a_s=m(1+2s\omega_c/m)^{1/2} \tag{5}$$

includes energy (or inertia) from both the rest mass, m, and the quantized cyclotron motion perpendicular to the field, $\omega_c=eB/m$. Electrons populate the system up to the Fermi energy ε_F, and each level is filled to a maximum value, p_s, of the momentum parallel to the field:

$$p_s=(\varepsilon_F^2-a_s^2)^{1/2}\ . \tag{6}$$

The Fermi energy can be determined from the density n by inverting the relation

$$n=\frac{eB}{2\pi^2}\left[p_0+2\sum_{s=1}^{s_F}p_s\right]\ , \tag{7}$$

where the sum extends over all s for which p_s is real.

Magnetic-field effects are more important at higher field strengths or at lower densities, where the magnetic-field-dependent Landau-level spacing is wider relative to the density-dependent Fermi energy. The scaling parameter for the magnetic field is $B_c=4.41\times10^{13}$ G, the field at which the cyclotron energy is equal to the electron rest-mass energy ($eB_c=m^2$, in our units). A characteristic density for the highly magnetized equilibrium system is the maximum density at which all electrons are in the lowest ($s=0$) Landau level:

$$n_0=1.244\times10^{30}(B/B_c)^{3/2}\ . \tag{8}$$

In the presence of a magnetic field, a photon can decay into an electron-positron pair. The electron and the positron in this pair can be created on the same or on different Landau levels, depending on the angular momentum (or polarization) of the initial photon. For parallel propagation within the medium, three photon

polarizations are possible: one longitudinal mode, which decays into two particles on the same level; transverse right-circular polarization, which decays into an electron on level s and a positron on level $s-1$; and transverse left-circular polarization, which decays into an electron on level s and a positron on level $s+1$.

The photon frequency ω and parallel momentum k are related to the electron and positron energy and momentum by energy and momentum conservation:

$$\omega=\varepsilon_{ps}+\varepsilon_{k-p,s'} , \tag{9}$$

where the electron has momentum p and is on level s, and the positron has momentum $k-p$ and is on level s'. In a vacuum, pair production is favored at values of the electron momentum p which minimize the pair energy in Eq. (9). This is evident from the behavior of the polarization tensor, described below. These minimum pair energies are

$$\omega_{\min}^{s,s'}=[(a_s+a_{s'})^2+k^2]^{1/2} , \tag{10}$$

where s and s' are related by the photon polarization:

$$s'=\begin{cases} s+1 & \text{for left-circular polarization} , \\ s & \text{for longitudinal polarization} , \\ s-1 & \text{for right-circular polarization} . \end{cases} \tag{11}$$

The electron and positron momenta at the minimum energy are $a_s k/(a_s+a_{s'})$ and $a_{s'}k/(a_s+a_{s'})$, and their velocities, p/ε_{ps} and $(k-p)/\varepsilon_{p-k,s'}$ are equal. At the $\omega_{\min}^{s,s'}$ values, both real and imaginary parts of $\Pi_{\mu\nu}^0(k,\omega)$ develop singularities. In a degenerate electron gas, however, the Pauli principle inhibits pair production when the electron momentum is less than the Fermi momentum for a particular Landau level [the created positron has no such restriction, and can be placed on any Landau level that satisfies Eq. (11)]. Thus, if the minimizing electron momentum is too low, it will not be possible to form a pair with energy $\omega_{\min}^{s,s'}$, and the structure at $\omega_{\min}^{s,s'}$ in the vacuum polarization tensor is completely canceled by the particle contribution to the polarization.

The energy of a pair [Eq. (9)] with the electron on the Fermi surface is qualitatively shown in Fig. 1, which has been drawn for $s=s'=0$ and chemical potential $\varepsilon_F=1.7$. There are two possible configurations: the $\omega_+^s(k)$ curve corresponds to electron momentum $+p_s$, and the $\omega_-^s(k)$ curve corresponds to electron momentum $-p_s$. Pair energies for electron momenta within the Fermi sea lie under the ω_-^s curve; as the electron momentum increases from $-p_s$ to $+p_s$, the pair energy decreases from ω_-^s and, for small k, reaches a minimum of $\omega_{\min}^{s,s'}$ [Eq. (10)] before increasing again to ω_+^s. For large k, however, the Fermi sea includes only the area between ω_-^s and ω_+^s. Qualitatively, the same picture prevails for the transverse modes ($s'=s\pm1$) also. The minimum pair energy $\omega_{\min}^{s,s'}$ is within the Fermi sea only for $k<k_{s,s'}$, where

$$k_{s,s'}\equiv\left|\frac{a_s+a_{s'}}{a_s}\right|p_s . \tag{12}$$

Thus, only for $k>k_{s,s'}$ is pair production possible at $\omega_{\min}^{s,s'}$. At $k=k_{s,s'}$, the $\omega_+^{s,s'}$ and $\omega_{\min}^{s,s'}(k)$ curves are tangent to each other.

The derivation of the particle $\Pi_{\mu\nu}(k,\omega)$ is sketched in the Appendix [1]. For $\mathbf{k}\|\mathbf{B}$, it has three independent elements, which at zero temperature are given by

$$\Pi_{33}(k,\omega)=-ie\sum_s\int_{-p_s}^{p_s}\frac{z_s(k,\omega)}{\omega\varepsilon_{ps}-pk-\frac{1}{2}(\omega^2-k^2)}dp , \tag{13}$$

$$\Pi_{\pm}(k,\omega)\equiv\Pi_{11}\pm i\Pi_{12}$$
$$=-ie\sum_s\int_{-p_s}^{p_s}\frac{x_s(k,\omega)\pm iy_s(k,\omega)}{\omega\varepsilon_{ps}-pk-\frac{1}{2}(\omega^2-k^2)\pm m\omega_c}dp , \tag{14}$$

where x_s, y_s, and z_s are analytic (k,ω)-dependent functions that are listed in the Appendix. This relativistic expression is similar to that of the more familiar classical response function [12]. The important features in the present context are the logarithmic divergences resulting from the roots of the denominators at the Fermi momentum, which are not found in the vacuum polarization. The integrals in Eqs. (13) and (14) have been evaluated

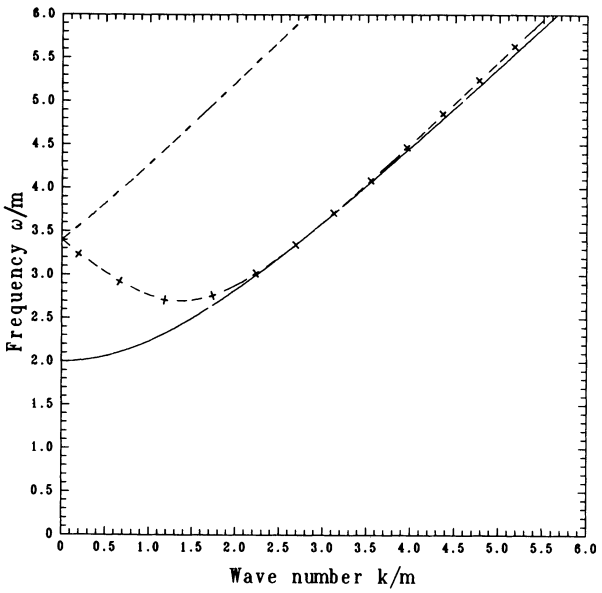

FIG. 1. Wave energy ω (in electron rest-mass units) vs wave number k (in inverse Compton wavelength units). Broken curves: Wave energy required to create an electron-positron pair when the electron is on the Fermi surface and originally moving with momentum p_s, either along the direction of the photon (the "+" curve) or opposite to the photon (the "−" curve). See Eq. (9). Solid bottom curve is the minimum energy required for an electron-positron pair. These curves are drawn for longitudinal polarization with $\varepsilon_F=1.7$ and $B=B_c$, corresponding to a density of $n=1.210\times10^{30}$ cm^{-3}; curves for other densities and for circular polarization will look similar. See Eq. (9).

analytically [1].

As an illustration of the high-frequency behavior of the polarization tensor, which is qualitatively the same for both longitudinal and transverse components of $\Pi(k,\omega)$, the real part of $4\pi\Pi_{33}(k,\omega)/\omega^2$ is plotted [1] in Fig. 2 for the case of $B=B_c$ and $\varepsilon_F=1.7$ (corresponding to a density $n=1.210\times10^{30}$ cm^{-3} and $p_0=1.375$), and for $k=4$, which is greater than the critical $k_{0,0}=2.75$. Evident in this figure are the negative-going vacuum peaks at $\omega_{\min}^{0,0}=4.47$, $\omega_{\min}^{1,1}=5.29$, and $\omega_{\min}^{2,2}=6.00$, as well as the positive-going peak at $\omega=4.51$ which arises from the denominator of Eq. (13), below. The imaginary part of $\Pi_{33}(k,\omega)$ is plotted in Fig. 3, for the same parameters; it is characterized by discontinuities at those points where the real part is divergent.

III. DISPERSION RELATION

The dispersion relation [Eq. (3)] separates into three equations, with three different polarizations of the resultant waves. Longitudinally polarized modes come from the solution of

$$4\pi\Pi_{33}(k,\omega)/\omega^2=1\ . \tag{15}$$

There are also two transverse-mode solutions, which come from the solutions of

$$\frac{4\pi\Pi_{\pm}(k,\omega)}{\omega^2-k^2}=1\ . \tag{16}$$

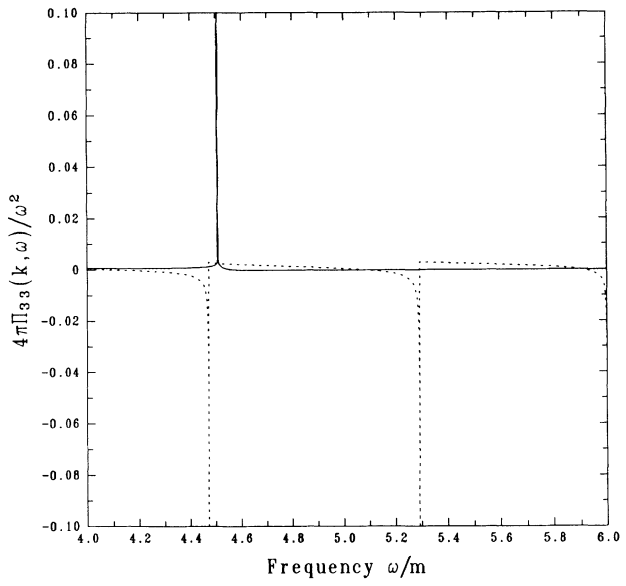

FIG. 2. Vacuum contribution (dashed line) and particle contribution (solid line) to the left-hand side of Eq. (15), $4\pi\Pi_{33}(k,\omega)/\omega^2$. This curve is drawn for $B=B_c$ and $\varepsilon_F=1.7$, corresponding to one occupied Landau level and a density of $n=1.210\times10^{30}$ cm^{-3}. The wave vector $k=4$, which is greater than the critical wave vector $k_{0,0}$; this large value has been chosen for clarity of display. Total polarization (real part) is the sum of vacuum and particle parts; a collective mode is predicted when the sum of these curves equals unity. The transverse polarization gives rise to a similar high-frequency graph.

These transcendental equations can be solved graphically or numerically for the, in general complex, frequency ω.

For frequencies $\omega>2m$ (the domain of interest), the amplitude of the left-hand side of Eqs. (15) and (16) is much smaller than one, except at isolated singularities (see Fig. 2), since $\Pi(k,\omega)$ decreases with increasing ω as ω^{-2}. The solutions to the dispersion equations are thus found near these singularities, which are found at the roots of the denominators of Eqs. (13) and (14) when $p=p_s$. For a given s value there are up to four such root frequencies ω_i, corresponding to different signs for the momentum and energy of the positron and of the electron: These include two "low" frequencies: $\omega_{l+}^{s,s'},\omega_{l-}^{s,s'}<2m$, and two "high" frequencies: $\omega_{h+}^{s,s'},\omega_{h-}^{s,s'}>2m$. The low frequencies are not considered here. The high frequencies turn out to be just those given by Eq. (9), and which are plotted in Fig. 1 for longitudinal modes (therefore we shall henceforth drop the "h" and refer to these as $\omega_{\pm}^{s,s'}$). At each root frequency there is a singularity of the form $\pm\ln(\omega-\omega_i^{s,s'})$ in the expression for $\Pi(k,\omega)$. If the logarithmic peak at $\omega_i^{s,s'}$ points upwards, the real part of the dispersion relation will have two solutions nearby, one at slightly less than $\omega_i^{s,s'}$ and one at slightly greater than $\omega_i^{s,s'}$. The imaginary part of the equation will generally only have one solution, which then determines the frequency and damping of the dispersion solution.

The polarization peaks at both of $\omega_{\pm}^{s,s'}$ point downwards at $k=0$, and so no mode exists there. However, when $k>k_{s,s'}$, the $\omega_{+}^{s,s'}$ peak switches direction and points upwards. When both real and imaginary parts of the dispersion equation are satisfied, a pair of propagating (but damped) modes are obtained, at a frequency that is very close to the peak frequency,

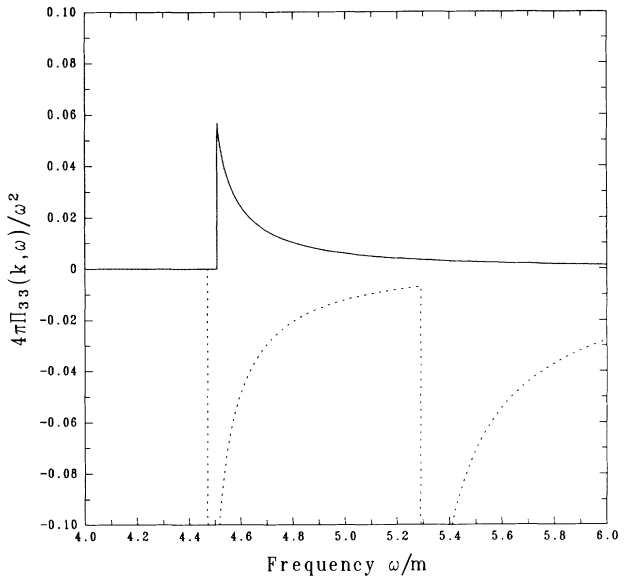

FIG. 3. Vacuum contribution (dashed line) and particle contribution (solid line) to the imaginary part of $\Pi_{33}(k,\omega)$. Same parameters were used as in Fig. 2. Discontinuities in $\mathrm{Im}[\Pi(k,\omega)]$ correspond to the divergences in $\mathrm{Re}[\Pi(k,\omega)]$.

$$\omega_{+}^{s,s'}=\varepsilon_F+[a_{s'}^2+(p_{s'}-k)^2]^{1/2} . \quad (17)$$

These are the pair modes that form the subject of this paper.

A new set of pair modes appears with each filled Landau level, since each level independently gives rise to a peak in the polarization tensor. In general, if s_F levels are occupied, there are s_F longitudinal and left-circularly polarized pairs and s_F-1 right-circularly polarized pairs of high-frequency solutions near the singularities at each $\omega_{+}^{s,s'}$.

The variation with k of the group velocity of the pair mode $\partial\omega_{+}^{s,s'}/\partial k$ can be seen from Fig. 1: Initially negative, the group velocity increases with increasing k, goes through zero, and becomes positive. When $k=k_{s,s'}$, the group velocity is just equal to the velocity of an electron on the Fermi surface; it thereafter continues to increase with k. The condition for wave propagation can thus also be expressed as

$$\frac{\partial\omega_{+}^{s,s'}}{\partial k}>\frac{p_s}{\varepsilon_F} . \quad (18)$$

The group velocity never exceeds the speed of light, although the phase velocity $\omega_{+}^{s,s'}/k$ is always superluminal.

Numerically obtained high-frequency solutions to the dispersion relations for longitudinal and left-circular polarizations are shown in Fig. 4 for the same parameters as in Fig. 1: Electron density 1.210×10^{30} cm^{-3} and $B=B_c$, for a Fermi energy $\varepsilon_F=1.7$ and Fermi-surface momentum for the only occupied Landau level $p_0/m=1.37$. There is no mode with right-circular polarization when only the lowest Landau level is occupied, because for this polarization the positron in the pair must be created on a lower Landau level than the electron, and the electron is already on the lowest possible level. A right-circular polarized mode does appear when higher Landau levels are occupied. Figure 5 illustrates this with a plot of the dispersion relation for a system with electron density 4.5×10^{30} cm^{-3} and $B=B_c$; here, the Fermi energy is $\varepsilon_F=2.24$, and there are three Landau levels occupied, with Fermi momenta $p_0/m=2.004$, $p_1/m=1.420$, and $p_2/m=0.133$.

The peaks in the real part of $\Pi(k,\omega)$ which give rise to these modes are extremely narrow, limiting frequency shifting due to damping and indicating a sensitivity to finite-temperature and collisional effects. The peak width near the dispersion solution can be estimated by assuming that, close to a singularity at $\omega_0(k)$,

$$\Pi(k,\omega)\approx A(\omega)\ln\frac{\omega+\omega_0}{\omega-\omega_0} , \quad (19)$$

where $A(\omega)>0$. This argument breaks down only for k near $k_{s,s'}$, where the peak is wider than predicted here (see below). Except in that case, the width $\Delta\omega=\omega-\omega_0$ is approximately

$$\Delta\omega\approx2\omega_0 e^{-\omega_0^2/4\pi A(\omega_0)} . \quad (20)$$

For longitudinal modes, for example,

$$A(\omega)=\frac{e^3B\sigma_s}{(2\pi)^2}\frac{a_s^2\omega^2}{(\omega^2-k^2)^{3/2}[(\omega^2-k^2)-4a_s^2]^{1/2}} , \quad (21)$$

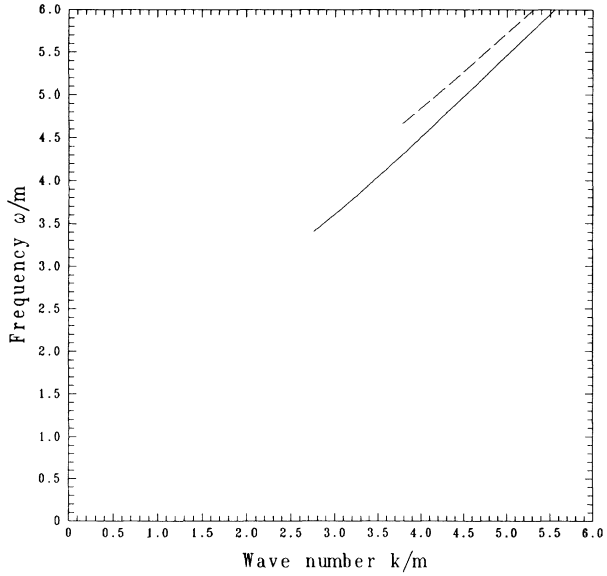

FIG. 4. Numerically determined dispersion relation $\omega(k)$ for $B=B_c$ and electron density $n=1.210\times10^{30}$ cm^{-3}. Dashed line is for left-circularly polarized modes, and solid curve is for longitudinally polarized modes. Units are the same as for Fig. 1. Since only one Landau level is occupied, there is no right-circularly polarized mode.

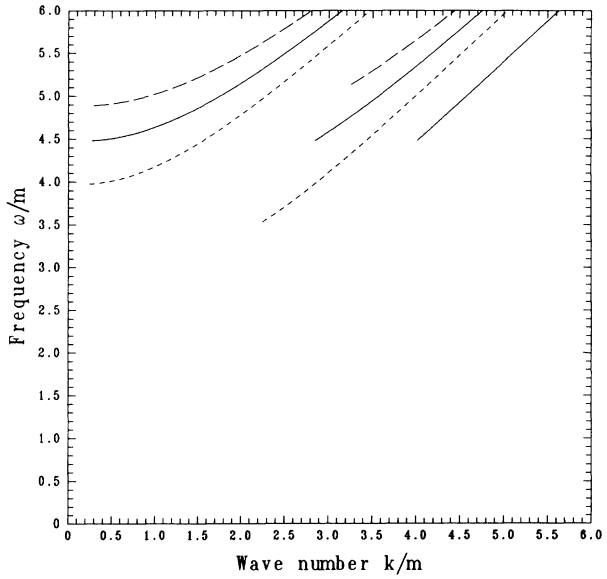

FIG. 5. Numerically determined dispersion relation $\omega(k)$ for $B=B_c$ and electron density $n=4.5\times10^{30}$ cm^{-3}. Three Landau levels are occupied, and so several modes are present for each polarization: Dashed lines are for left circular polarization (LCP), dotted lines are for right circular polarization, and longitudinal polarization is shown by solid lines. The LCP mode from the lowest Landau level turns on at $k=5.48$, $\omega=6.12$ and so is off the scale.

where

$$\sigma_s \equiv \begin{cases} \frac{1}{2} & \text{if } s=0 \ , \\ 1 & \text{otherwise} \ . \end{cases} \tag{22}$$

A similar expression holds for the transverse modes. Except near $k_{s,s'}$, where it diverges as $(k-k_{s,s'})^{-1}$, $A(\omega_0)/\omega_0^2$ is very small, being proportional to e^2B/B_c. The peaks are so narrow that the equation for the center of the peak, Eq. (17), is effectively the dispersion relation.

Pair modes are strongest for $k \approx k_{s,s'}$, because the mode-generating peak is broadest there and because, as will be shown, damping is weakest there. The method of Eq. (19) cannot be used near the critical wave number, because ω_0 approaches zero and $A(\omega)$ diverges at $k_{s,s'}$; instead, both $A(\omega)$ and the argument of the logarithm are expanded in the small quantity $\kappa \equiv k-k_{s,s'}$, and the small-κ limit is investigated. The result for longitudinal modes and small but nonzero κ is

$$\Delta\omega \approx \frac{e^3B}{\pi}\frac{\sigma_s}{2\varepsilon_F^2}\kappa \ . \tag{23}$$

When $\kappa=0$, the peak width is actually nonzero, but very small. The width increases with κ until it reaches a maximum value of

$$\Delta\omega_{\max}=0.1055\left[\frac{e^3B\sigma_s}{\pi}\right]^2\frac{1}{a_s^2\varepsilon_F} \tag{24}$$

at

$$\kappa_{\max}=1.06\frac{e^3B\sigma_s}{\pi}\frac{\varepsilon_F}{a_s^2} \ , \tag{25}$$

after which the peak rapidly narrows. The transverse peaks exhibit similar behavior.

To study damping of the pair-production modes, the behavior of the complex vacuum and particle polarization tensors must be known. We again use the longitudinal mode as an example; the transversely polarized modes are more complicated, but exhibit no new features. For the longitudinal polarization, the k-ω plane is divided into different regions, as shown in Fig. 6. The boundaries to these regions, at which there can be a discontinuous change in $\mathrm{Im}[\Pi(k,\omega)]$, are the Fermi-surface singularity frequencies $\omega_+^{s,s'}$ and $\omega_-^{s,s'}$, the minimum pair-creation frequency $\omega_{\min}^{s,s'}$, and the $\omega=k$ line, below which is the low-frequency regime [1] not considered here.

Region A in Fig. 6 is a transparency region, where both particle and vacuum contributions to $\mathrm{Im}[\Pi(k,\omega)]$ are zero, since no value of electron momentum gives a pair energy less than $\omega_{\min}^{s,s}$. There is also zero damping in region B, where $k<k_{s,s}$ and $\omega<\omega_+^{s,s}$, because the vacuum peak at $\omega_{\min}^{s,s}$ is exactly cancelled by the particle contribution. In region C, partial cancellation occurs: $\mathrm{Im}[\Pi(k,\omega)]$ is reduced by the particle contribution to half the vacuum level. In region D, where $k>k_{s,s}$, there is no cancellation, the created pair lies outside the Fermi

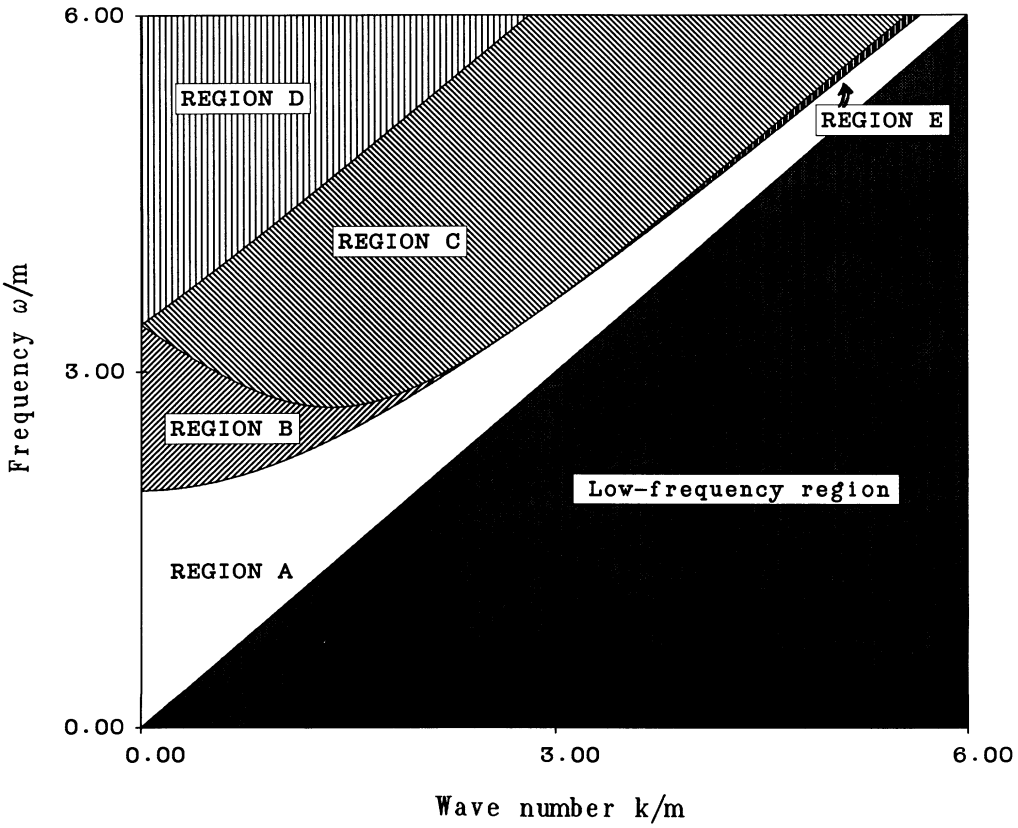

FIG. 6. Regions of different dispersion in the ω-k plane. See text for discussion. The dividing lines are the Fermi surface and minimum-energy lines shown in Fig. 1. The same parameters are used as for Fig. 1. For this figure, $k_s=2.75$ and $\omega(k_s)=3.4$.

surface, and the full (weak) vacuum damping occurs. This is also true in region E, where there is the full (strong) vacuum damping. The pair modes discussed here are located on either side of the boundary line $\omega_+^{s,s}$ separating regions C and E.

Clearly, damping of the high-frequency modes is due to the vacuum polarization. It is the nonzero imaginary part of the vacuum-polarization tensor above the pair-production threshold $\omega_{\min}^{s,s'}$ which prevents the dispersion equation from having an undamped solution, with a purely real ω. The particle contribution partially cancels the vacuum contribution above $\omega_+^{s,s'}$, by eliminating one of two possible channels of the pair-creation process, but below $\omega_+^{s,s'}$ the particle contribution is zero, and nowhere in the mode-propagation region can the particles eliminate the vacuum damping. Thus, the damping mechanism is just what it would have been in the absence of the particles, although it is reduced: it is pair production, which converts wave energy into a flux of particles. (This is analogous to the description of low-frequency Landau damping as a decay into electron-hole pairs [12].)

The damping coefficient $\gamma=-\mathrm{Im}(\omega)$ of the modes can be calculated as

$$\gamma=\sigma\pi\left[\frac{\partial}{\partial\omega}\frac{A(\omega)}{\omega^2}\right]^{-1}, \tag{26}$$

where $\sigma=1$ for $\Delta\omega>0$ and $\sigma=2$ for $\Delta\omega<0$. It is given, for longitudinal polarization, by

$$\gamma_s=\frac{\sigma\sigma_s m^2e^2}{\omega_+}\frac{B}{B_c}\left[\frac{a_s^2}{\omega_+^2-k^2}\right]\times\left[\frac{[1-4a_s^2/(\omega_+^2-k^2)]^{1/2}}{1-3a_s^2/(\omega_+^2-k^2)}\right]. \tag{27}$$

An order-of-magnitude estimate of the damping can be found from the limit of Eq. (27) for small p_s and $k_{s,s}$:

$$\gamma_s(p_s\ll a_s)\approx\frac{m^2e^2B\sigma}{2a_s^2B_c}\left[p-\frac{k}{2}\right]. \tag{28}$$

From this, it can be readily seen that γ_s is small for a large range of k values, compared to $\omega_+^{s,s'}\approx 2\varepsilon_F$.

A plot of $\gamma_0(k)$ is given in Fig. 7 for the same parameters as in Fig. 5. Damping is close to zero at $k_{s,s}$, increases rapidly to a maximum value roughly proportional to the Fermi momentum p_s, and then slowly decreases. At its maximum, the decay time is about 10^{-18} sec in Fig. 7, or about 10^4 times the real part of ω^{-1}.

Additional damping would be expected from temperature and collisional effects not included in the model discussed here. These effects could prevent the propagation of the mode if the temperature or collisional-damping coefficient is comparable to or greater than the peak width $\Delta\omega$.

Another way of assessing the importance of the pair modes is by evaluating their contribution to the density and current fluctuations. The contribution to the density fluctuations can be estimated by considering the f-sum rule, which requires that the integral of the imaginary part of the reciprocal of the dielectric function be constant:

$$\int_0^\infty d\omega\,\omega\,\mathrm{Im}\frac{1}{\epsilon(k,\omega)}=\text{const}. \tag{29}$$

[In the nonrelativistic limit, this constant is $(\pi/2)\omega_p^2$, where $\omega_p=(4\pi ne^2/m)^{1/2}$ is the plasma frequency.] The portion which the integral on the right-hand of Eq. (29) picks up by integration through the pair-mode pole [where $\epsilon(k,\omega)$ has a zero] can be estimated through simple algebra to be of the order $\omega_0\Delta\omega$. Using the results of Eq. (24), the maximum value of the right-hand integral can be found for longitudinal polarization, when only the $s=0$ level is occupied; the maximum pair-mode contribution to the sum-rule integration is then

$$\max\left\{\int_{\substack{\text{pair}\\\text{modes}}}d\omega\,\omega\,\mathrm{Im}\frac{1}{\epsilon(k,\omega)}\right\}\approx 0.036\left[\frac{e^3B}{\pi a_s}\right]^2. \tag{30}$$

By contrast, the plasma frequency is limited when only the lowest level is occupied to be

$$\omega_p^2\le 2.83\frac{e^2}{\pi}(eB)^{3/2}. \tag{31}$$

The pair-mode contribution of Eq. (30) is small compared to this maximum ω_p^2 value, except for ultrastrong magnetic fields ($B>B_c/e^4$). The pair-mode contribution is not negligible, however, especially at densities below the maximum level-filling density.

The formula (20) for $\Delta\omega$ has the nonanalytic exponential dependence on A characteristic of the Cooper phenomenon [3,4] where $\Delta\omega\sim e^{-1/N_0V}$; here, the density of states per unit volume at the Fermi surface, N_0, is represented by eB, as is typical in a highly degenerate

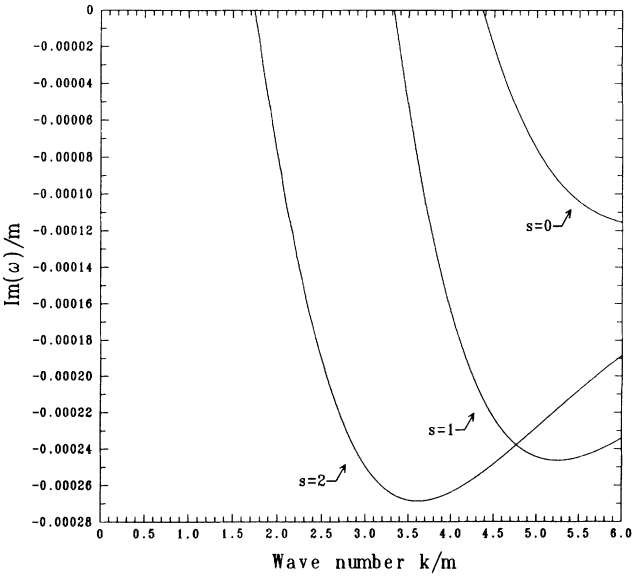

FIG. 7. Damping, in units of $mc^2/\hbar=7.76\times10^{20}$ sec^{-1}, for the same case as Fig. 5. One curve arises from each occupied Landau level in the system, as noted.

magnetized system, while the average interaction strength V is of order e^2/m^2, with m^{-1} playing the role of the "range" of the virtual electron-positron pair interaction. This explains why $\Delta\omega$, the strength of the excitation, becomes extremely small when B deviates substantially from the ultrastrong value $B_c/e^2 \approx 604\times 10^{13}$ G. The situation, however, is quite different in the vicinity of the critical point where $k \approx k_{s,s'}$ and $\omega \approx \omega_{\min}^{s,s'}$, where $A(\omega)$ has a $(\omega^2-\omega_{\min}^{s,s'2})^{-1/2}$ singularity. In this case the width reaches a maximum, given by Eq. (24), which avoids the drastic collapse of the excitation strength away from $k_{s,s'}$.

IV. VALIDITY

The theory presented here is limited primarily by three assumptions. First, as has been seen, the assumption of low temperature places a lower limit on the electron density; if only the zero Landau level is occupied, this restriction can be expressed as

$$n > 4.6\times 10^{21}(kT)^{3/2}\ \text{cm}^{-3} \tag{32}$$

with kT in eV. Higher Landau levels, with smaller Fermi momenta, will be even more susceptible to thermal distortions. However, the most severe restriction on the temperature comes from the condition that temperature broadening may not be much larger than the peak width $\Delta\omega$.

The density is limited by the assumption of weak interparticle interaction. For the random-phase approximation (RPA) to be valid, the correlation energy should be much less than the Fermi kinetic energy; this places a corresponding condition on the conventional coupling parameter

$$r_s \equiv (3/4\pi n)^{1/3}/a_B\ , \tag{33}$$

where a_B is the Bohr radius. While for a system of many filled levels the condition $r_s \ll 1$ is appropriate, for a strongly magnetized system a stricter condition applies. If only the lowest Landau level is occupied, then it must be true that [from Eq. (8)]

$$r_s > 1.49 l/a_B = 1.49 e^2/(B/B_c)^{1/2}\ , \tag{34}$$

where the magnetic length is $l = 1/\sqrt{eB}$. If in addition the system is nonrelativistic ($p_0 \ll m$), the weak-coupling condition is

$$r_s < 1.62(l/a_B)^{4/5} = 1.62\left[\frac{e^4}{B/B_c}\right]^{2/5}\ . \tag{35a}$$

This nonrelativistic condition applies to all but ultramagnetized systems ($B > 5\times 10^7 B_c$); for these, the minimum weak-coupling Fermi momentum $p_0 \gg m$, and the ultrarelativistic condition

$$r_s < \frac{2.17}{(e^2)^{1/2}}(l/a_B) = 2.17\left[\frac{e^2}{B/B_c}\right]^{1/2} \tag{35b}$$

must be used. The various domains of relativistic corrections and degree of coupling for electrons on the Fermi surface are shown in Fig. 8 as a function of magnetic field and coupling parameter r_s, together with the boundary of the region where only the zero Landau level is occupied, Eq. (34). If the density is higher than Eq. (8), so that more levels are occupied, Eqs. (35) are automatically satisfied (assuming that $r_s < 1$), and the lowest level is certainly weakly coupled. The strongest coupling is experienced by the highest Landau levels, which even in a dense system can have near-zero parallel momentum p_s. One should note, however, that the condition of low correlation energy is only a requirement for the validity of the RPA, and not for the existence of the pair modes. Indeed, the pair binding should be enhanced in higher-order perturbation calculations, thus making the pair modes actually more robust [4].

One expects the breakdown of the RPA to be nonuniform, and to occur first for short wavelengths. We have assumed the perturbation wavelength to be no shorter than the interparticle separation; this should limit the mode wave number to $k < n^{1/3}$. For large wave numbers, the mode probably broadens and damps by higher-order processes; the damping γ is expected to increase with k beyond the maximum value predicted by Eq. (27). The limitation on k does not preclude the appearance of the pair-production mode, since k can be as small as the critical wave number, $k_{s,s'}$, and $k_{s,s'}$ can be nearly zero for a

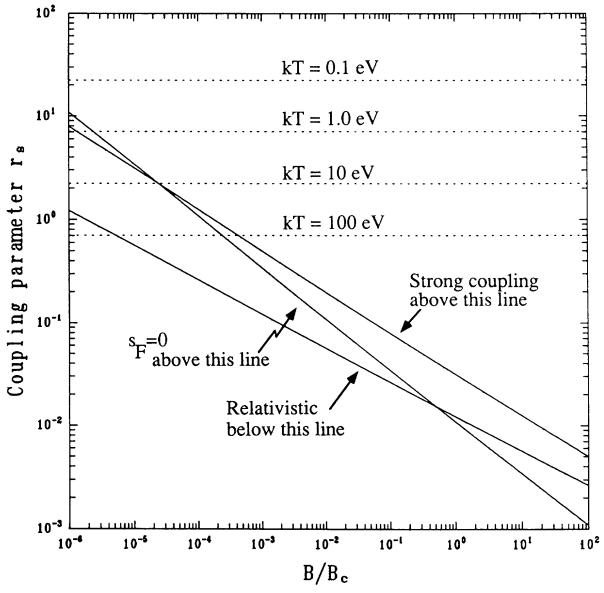

FIG. 8. Degree of coupling and importance of relativity in the dynamics of Fermi-surface electrons, as a function of magnetic field B/B_c and the coupling parameter r_s, which is the mean interparticle separation divided by the Bohr radius. The three solid lines are Eq. (35a), below which the RPA weak-coupling approximation is good; Eq. (34), above which all electrons are in the zero Landau level; and $r_s = 1.6765\ e^2/(B/B_c)^{1/3}$, below which the Fermi-surface electrons are relativistic. Also shown as dashed horizontal lines are the r_s values solving Eq. (32) for temperatures of 0.1, 1.0, 10, and 100 eV; the zero-temperature approximation for the zero Landau level holds good only below these lines (for higher levels, the temperature condition is stricter).

sparsely filled level. Still, this limitation does mean that the mode is most likely to be seen on the highest Landau level.

V. CONCLUSIONS

In summary, we have seen that pair-production modes with frequencies

$$\omega^{s,s'}(k) \approx \varepsilon_F + [a_{s'}^2 + (p_s - k)^2]^{1/2} \tag{36}$$

can propagate along the magnetic field in an electron gas, if the parallel wave vector satisfies $k > k_{s,s'}$. The modes are damped by pair creation, but within the limits of the present theory (the RPA), damping is not significant. The pair-production mode can have any of the three polarizations permitted by the symmetry of the problem (subject to momentum-conservation requirements).

The critical wave number $k_{s,s'}$, defined in Eq. (12), is the point above which the mode group velocity exceeds the velocity of an electron on the Fermi surface of Landau level s, and is also the lowest mode momentum for which an electron-positron pair can be created with the minimizing energy $\omega_{\min}^{s,s'}$ [see Eq. (10)]. When $k = k_{s,s'}$, the electron and positron of a created pair would have their greatest degree of interaction: they would be stationary with respect to each other.

Interaction between the virtual electron and positron in the pair is enhanced by the Cooper phenomenon, where the background degenerate electron gas reduces the momentum space available for the electron. This situation resembles a Mahan exciton [4], where an electron emerges above the Fermi surface from a deep-lying core state, and binds to the hole that was left behind. In Mahan's calculation [4], a logarithmic singularity appears in the lowest-order evaluation of $\Pi(k,\omega)$; however, summation of higher-order ladder diagrams leads to the replacement of the logarithmic singularity by an inverse-power singularity in the vicinity of the mode frequency. One may speculate about the possibility of a similar phenomenon in the present case, as a result of enhancements to the pair binding from post-RPA-type contributions to the polarization which have been ignored in the present calculations.

The results presented here include the presence of a strong background magnetic field, but pair modes similar to those described here might also be found in an unmagnetized system. The very weak effective interaction described here between the virtual electron and positron ordinarily mandates a very high density of states on the Fermi surface, to avoid an exponentially low excitation strength; and since the density of states is proportional to B, an ultrastrong field strength, of order $e^{-2}B_c$, is normally required. The situation is different for $k \sim k_{s,s'}$, however, where a strong and possibly even observable effect can exist for lower magnetic-field values. As the density is increased or the magnetic field is decreased, the mode wavelength for lower Landau levels becomes smaller than the interparticle spacing, and the mode probably vanishes; at the same time, however, higher Landau levels are populated, and the mode reappears from the higher levels. If not for the short-wavelength limitations on the theory, the discrete modes of Figs. 4 and 5 would increase in number and decrease in separation at smaller magnetic fields, perhaps merging into a propagation band. In the magnetic-field-free situation, the kinematics of electron-positron pair creation with a relativistic Fermi sphere of electrons is similar to what has been described here, as is demonstrated by the structure of the relativistic (zero-field) $\Pi(k,\omega)$ [13]. The density of states on the Fermi surface is then of order p_F^2, and can reach a sufficiently high value for $n \sim (e^2)^{-3/2} m^{-3}$, about 10^{34} cm^{-3}, which is not excessively high. The real question is whether the logarithmic singularity generating the mode survives for high wave numbers in the three-dimensional case, as it does in the one-dimensional system. This cannot be determined without further work.

The phenomenon we describe here, in addition to generating a mode of collective oscillation, affects the structure of the polarization tensor $\Pi_{\mu\nu}(k,\omega)$, and so leads to other physical effects. In particular, the optical properties of a relativistic, magnetized electron gas would be strongly modified in the vicinity of the mode frequency through the appearance of a sharp, magnetic-field- and density-dependent absorption-emission edge. This may prove to be the most promising observational consequence of the phenomenon.

ACKNOWLEDGMENT

This work has been partially supported by NSF Grant No. ECS-87-13337.

APPENDIX: BRIEF DERIVATION OF THE POLARIZATION TENSOR

A first-order quantum-relativistic kinetic theory [1,5] was used to derive an expression for the polarization tensor $\Pi_{\mu\nu}(k,\omega)$. This derivation is sketched here; the details have been given elsewhere [1]. The notation used here is the same as in the text: The Minkowskian metric tensor has the signature $(1,-1,-1,-1)$, and the Einstein summation convention is used. An electromagnetic perturbation to the system is represented by the four-potential A_μ, and the system response is given by the Wigner distribution function $F_{ij}(x,p)$, defined in terms of the field operators of the system (the subscript indices on F_{ij} are spinor-matrix indices). Fortunately, it is not necessary to find the complete matrix F_{ij} to determine the perturbed current and so the polarization tensor; the current is given directly by the integral of the vector distribution function $f_\mu(x,p) = \mathrm{Tr}[\gamma_\mu F_{ij}(x,p)]$.

The vector distribution function is obtained from the linearized quantum Vlasov equation, which is Fourier transformed, assuming that the equilibrium distributions are uniform in space. In the electron rest frame, where there is no background electric field and the background magnetic field is in the $\hat{\mathbf{e}}_3$ direction, the only nonzero components of the field tensor are $F_{21} = -F_{12} = B$, and the vector distribution function obeys the differential equation

$$2p_\alpha \mathcal{L}^\alpha f_\mu + 2eF_{\alpha\mu} f^\alpha = \mathcal{L}^\alpha a_{\alpha\mu} + 2ap_\mu \ , \tag{A1}$$

where

$$\mathcal{L}^{\mu}\equiv ik^{\mu}+eF^{\alpha\mu}\frac{\partial}{\partial p^{\alpha}} \tag{A2}$$

and a and $a_{\alpha\mu}$ are terms from the spinor-space expansion of the Vlasov equation that depend on the equilibrium distribution functions and are linearly dependent on A_{μ}. The equilibrium distribution functions for a uniform highly magnetized electron gas are

$$f_{(0)}(p)=\frac{2m}{(2\pi)^3}e^{-\lambda^2 p_{\perp}^2}\left[\frac{1}{\varepsilon_{p0}}\frac{\delta(p_0-\varepsilon_{p0})}{e^{\beta(\varepsilon_{p0}-\mu)}+1}+\sum_{s=1}^{s_F}\frac{(-1)^s}{\varepsilon_{ps}}\frac{\delta(p_0-\varepsilon_{ps})}{e^{\beta(\varepsilon_{ps}-\mu)}+1}[L_s(2\lambda^2 p_{\perp}^2)-L_{s-1}(2\lambda^2 p_{\perp}^2)]\right], \tag{A3}$$

$$f^{\alpha}_{5(0)}=\frac{2i}{(2\pi)^3}\mathcal{P}^{\alpha}e^{-\lambda^2 p_{\perp}^2}\left[\frac{1}{\varepsilon_{p0}}\frac{\delta(p_0-\varepsilon_{p0})}{e^{\beta(\varepsilon_{p0}-\mu)}+1}+\sum_{s=1}^{s_F}\frac{(-1)^s}{\varepsilon_{ps}}\frac{\delta(p_0-\varepsilon_{ps})}{e^{\beta(\varepsilon_{ps}-\mu)}+1}[L_s(2\lambda^2 p_{\perp}^2)+L_{s-1}(2\lambda^2 p_{\perp}^2)]\right] \tag{A4}$$

where $\beta=(kT)^{-1}$, $\lambda^2=1/|eB|$, $L_s(x)$ is the Laguerre polynomial, μ is the chemical potential, and the four-vector $\mathcal{P}^{\mu}=(p_3,0,0,-p_0)$. At zero temperature, of course, each term in the sums becomes proportional to $\Theta(\varepsilon_F-\varepsilon_{ps})$, where ε_F is the Fermi energy.

The differential equation for f_{μ}, Eq. (A1), can be solved by a relativistic analog of the nonrelativistic "integral-over-unperturbed-orbits" procedure. The resulting integral expression for f_{μ} is not easily evaluated, but it may be further integrated to obtain the perturbed current and so, by identifying coefficients of A_{μ}, the polarization tensor [cf. Eq. (1)]. The magnetic field actually simplifies the procedure, for although an integrated expression for f_{μ} can be easily found for the unmagnetized plasma, carrying out the integrations to obtain the unmagnetized j_{μ} from this expression is quite difficult.

If only propagation parallel to the magnetic field is considered, there are only three independent elements of the polarization tensor, which can be taken to be $\Pi_{33}(k,\omega)$ and $\Pi_{\pm}(k,\omega)\equiv\Pi_{11}(k,\omega)\pm i\Pi_{12}(k,\omega)$. These are given by the Vlasov theory outlined here as

$$\Pi_{33}(k,\omega)=-ie\sum_s\int\frac{z_s}{(\varepsilon_{ps}-\omega/2)\omega-p_{\parallel}k_{\parallel}}d^4p\ , \tag{A5}$$

$$\Pi_{\pm}(k,\omega)=-ie\sum_s\int\frac{x_s\pm iy_s}{(\varepsilon_{ps}-\omega/2)\omega-p_{\parallel}k_{\parallel}\pm\omega_c}d^4p\ , \tag{A6}$$

where

$$x_s=\frac{ie}{2m}\omega\varepsilon_{ps}S_s+\frac{ie}{2m}k\left[p_3S_s-\frac{k}{2}D_s\right]-ise\omega_c D_s\ , \tag{A7}$$

$$y_s=\frac{ie}{2}(\omega D^3_{5s}+kD^0_{5s})+\frac{se^2B\omega_c}{p_{\perp}^2}\left[p_{\perp}\frac{\partial S_s}{\partial p_{\perp}}-S_s\right], \tag{A8}$$

$$z_s=-\frac{ie}{2m}\omega\varepsilon_{ps}S_s-\frac{ie}{m}p_3\left[p_3D_s-\frac{k}{2}S_s\right], \tag{A9}$$

and S_s, D_s, and D^{μ}_{5s} signify the sum (S) and difference (D) of the sth term in the Landau-level expansion of the equilibrium distribution functions:

$$S\equiv f_{(0)}(p+k/2)+f_{(0)}(p-k/2)\ , \tag{A10}$$

$$D\equiv f_{(0)}(p-k/2)-f_{(0)}(p+k/2)\ ,$$

$$D^{\mu}_5\equiv f^{\mu}_{5(0)}(p-k/2)-f^{\mu}_{5(0)}(p+k/2)\ . \tag{A11}$$

The expressions of Eqs. (A5) and (A6) are identical to Eqs. (13) and (14) in the main text.

*Present address: Radiation Hydrodynamics Branch, Code 4720, Naval Research Laboratory, Washington, DC 20375.

[1] Peter Pulsifer, Ph.D. dissertation, Boston College (1987); P. Pulsifer and G. Kalman, Bull. Am. Phys. Soc. **32**, 1726 (1987).
[2] R. A. Cover and G. Kalman, Phys. Rev. Lett. **33**, 1113 (1974).
[3] H. A. Bethe and J. Goldstone, Proc. R. Soc. London, Ser. A **238**, 551 (1957).
[4] G. D. Mahan, Phys. Rev. **152**, 882 (1967); **163**, 612 (1967).
[5] Horatio D. Sivak, Ann. Phys. (N.Y.) **159**, 351 (1985).
[6] H. Perez-Rojas and A. E. Shabad, Ann. Phys. (N.Y.) **138**, 1 (1982).
[7] P. Bakshi, R. Cover, and G. Kalman, Phys. Rev. D **14**, 2532 (1976).
[8] R. Cover, G. Kalman, and P. Bakshi, Phys. Rev. D **20**, 3015 (1979).
[9] B. Jancovici, Nuovo Cimento **25**, 428 (1962).
[10] A. E. Delsante and N. E. Frankel, Ann. Phys. (N.Y.) **125**, 135 (1980).
[11] V. Kowalenko, N. E. Frankel, and K. C. Hines, Phys. Rep. **126**, 109 (1985).
[12] D. Pines and P. Nozières, *The Theory of Quantum Liquids* (Benjamin, New York, 1966).
[13] G. Kalman, Bull. Am. Phys. Soc. **12**, 777 (1967); B. Prasad and G. Kalman, *ibid.* **13**, 309 (1968); G. Kalman and B. Prasad, Bull. Am. Astron. Soc. **1**, 195 (1969).

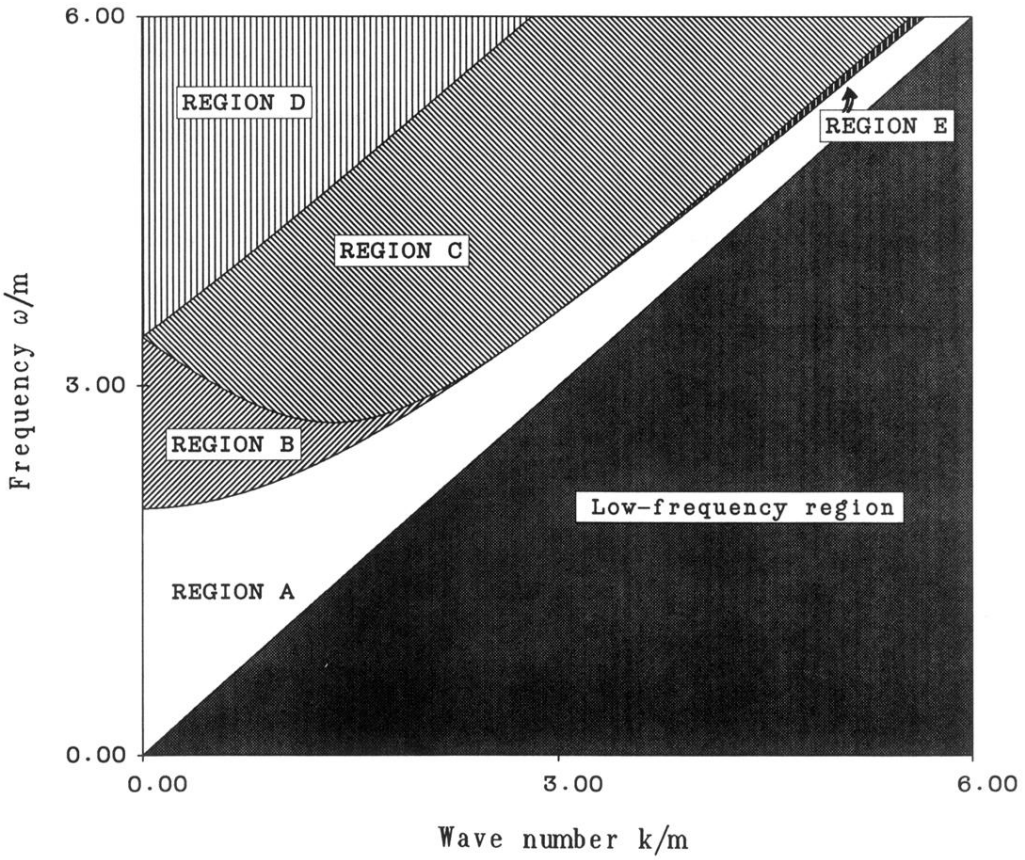

FIG. 6. Regions of different dispersion in the ω-k plane. See text for discussion. The dividing lines are the Fermi surface and minimum-energy lines shown in Fig. 1. The same parameters are used as for Fig. 1. For this figure, $k_s = 2.75$ and $\omega(k_s) = 3.4$.